A New Delayless Subband Adaptive Filtering Algorithm for Active Noise Control Systems

Ali A. Milani, *Student Member, IEEE*, Issa M. S. Panahi, *Senior Member, IEEE*, and Philipos C. Loizou, *Senior Member, IEEE*

***Abstract*—Subband adaptive filtering (SAF) techniques play a prominent role in designing active noise control (ANC) systems. They reduce the computational complexity of ANC algorithms, particularly, when the acoustic noise is a broadband signal and the system models have long impulse responses. In the commonly used uniform-discrete Fourier transform (DFT) -modulated (UDFTM) filter banks, increasing the number of subbands decreases the computational burden but can introduce excessive distortion, degrading performance of the ANC system. In this paper, we propose a new UDFTM-based adaptive subband filtering method that alleviates the degrading effects of the delay and side-lobe distortion introduced by the prototype filter on the system performance. The delay in filter bank is reduced by prototype filter design and the side-lobe distortion is compensated for by oversampling and appropriate stacking of subband weights. Experimental results show the improvement of performance and computational complexity of the proposed method in comparison to two commonly used subband and block adaptive filtering algorithms.**

***Index Terms*—Active noise control (ANC), discrete Fourier transform (DFT), filter bank, subband adaptive filter.**

I. Introduction

ACTIVE noise control (ANC) is a method of cancelling a noise signal in an acoustic cavity by generating an appropriate anti-noise signal via canceling loudspeakers. Due to recent advances in wireless technology, new applications of ANC have emerged, e.g., incorporating ANC in cell phones, Bluetooth headphones, and MP3 players, to mitigate the environmental acoustic noise and therefore improve the speech and music quality. For practical purposes, ANC as a real-time adaptive signal processing method should meet the following requirements: 1) minimum computational complexity (lower computational delay and power consumption), 2) stability and robustness to input noise dynamics, and 3) maximum noise attenuation.

Manuscript received August 13, 2008; revised January 12, 2009. Current version published June 10, 2009. This work was supported in part by a subcontract from UT Southwestern Medical Center at Dallas, funded by the Department of Veterans Affairs through VA IDIQ contract number VA549-P-0027 awarded and administered by the Dallas, TX, VA Medical Center. The content of this paper does not necessarily reflect the position or the policy of the Veterans Administration or the Federal government, and no official endorsement should be inferred. The associate editor coordinating the review of this manuscript and approving it for publication was Prof. Stephen J. Elliott.

The authors are with the Department of Electrical Engineering, University of Texas at Dallas, Richardson, TX 75080 USA (e-mail: ali.a.milani@student.utdallas.edu; issa.panahi@utdallas.edu; loizou@utdallas.edu).

Digital Object Identifier 10.1109/TASL.2009.2015691

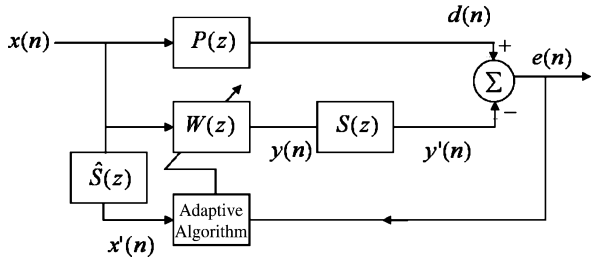

Fig. 1. Feed-forward FxNLMS algorithm, where $\hat{S}(z)$ is an estimate of $S(z)$.

Acoustical and electrical signal transmission path models such as those encountered in realistic ANC applications, e.g., the primary path $P(z)$ and the secondary path $S(z)$ (see Fig. 1), usually have long impulse responses [1], [2]. Consequently, noise cancellation algorithms require long adaptive filters, resulting in significant computational burden. The computational complexity can be reduced by using frequency-domain filtering techniques based on decomposition, processing, and reconstructing the signals using filter banks such as subband adaptive filtering (SAF) and block adaptive filtering (BAF) techniques. SAF techniques have been used in other audio applications such as speech enhancement and hearing aids [3]–[5]. Among the SAF methods [1], [6], [7], the delayless SAF introduced by Morgan and Thi (MT) in [1] provides a better approach to meet the aforementioned requirements for ANC system. Merched and Sayed [2] introduced a BAF algorithm named discrete Fourier transform multidelay adaptive filter (DFT-MDF). This algorithm exploits the properties of circulant matrices to implement a high-performance block adaptive processing algorithm. DFT-MDF (as it will be shown later) performs well with a small block lengths (or small number of subbands).

Zhou *et al.* [8] proposed an ANC system that requires no secondary path identification, whereby to cancel a single tone at frequency ω_k, the adaptive filter, denoted by $W(\omega_k)$ (see Fig. 1), needs to estimate the ratio of $P(\omega_k)/S(\omega_k)$ not $P(\omega_k)$ and $S(\omega_k)$ individually, and the phase is set to either 0° or 180° by trial and error. Expanding on this concept, [8] shows that a non-tonal noise signal can be canceled by decomposing it into very narrow subbands and treating each subband like a tonal component. According to [8], the narrower the subbands are, i.e., the higher the number of subbands, the better should be the performance of the system. Hence, an appropriate SAF technique with a large number of subbands may be used to avoid secondary path identification. The BAF algorithms are not suitable for this purpose since the adaptive filters within do not directly operate in subbands; they are used when a good estimate of the

secondary path is available. As we will show, the performance of BAF techniques deteriorates for a large number of subbands. Consequently, not only is a good estimate of the secondary path required, but the reduction of computational complexity is also limited by the small number of subbands.

In general, the SAF methods offer a good alternative approach to meet ANC system requirements, due to their inherent spectral decomposition and downsampling operations. Since the spectral dynamic range and eigenvalue spread of the covariance matrix of noise signal decrease in each subband, the performance, i.e., convergence rate, noise attenuation level, and stability of the ANC system, improves using SAF techniques [9]. Hence, one expects that increasing the number of subbands (or block length) M should improve the performance.

The delayless SAF scheme in an ANC system involves the decomposition of input noise (i.e., the reference signal) and error signals into subbands using analysis filter banks, and combining the subband weights into a full-band noise canceling filter by a synthesis filter bank called weight stacking. Typically, a linear-phase finite-impulse response (FIR) low-pass filter (i.e., prototype filter) is designed and modulated for the design of such filter banks [10]. The filter must be designed so that the side-lobe effect and spectral leakage are minimized. The latter requires a high-order FIR filter, introducing a long delay, which increases with M as the bandwidth shrinks. The long delay and side-lobe interference introduced by the prototype filter degrade the performance of SAF algorithms for large M, limiting the computational saving that can be obtained by increasing the number of subbands [2]. Improving the system performance and reducing the computational burden by increasing M has inspired the work presented herein.

In this paper, we first demonstrate that the increased delay degrades the system performance more than that of the spectral leakage (or side-lobe effects) in a uniform subband filtering method. It is shown how the spectral leakage can be reduced by choosing a proper decimation factor and weight stacking methodology. We then present a new SAF algorithm that reduces computational complexity by increasing the number of subbands M without degrading the performance of the ANC system. The performance of the proposed method is compared with those of MT and DFT-MDF methods in [1] and [2]. The results show that the maximum noise attenuation level (NAL) of the proposed method is higher than that of MT and comparable to that of the DFT-MDF method. However, the new method achieves the maximum NAL with much lower computational complexity and higher robustness than the other two methods.

This paper is organized as follows. Section II defines the notation and definitions used in the paper. The general structure of delayless subband adaptive filtering algorithm and the performance limiting factors of the MT algorithm are discussed in Section III. In Section IV, we present the new subband adaptive filtering method. Performance comparison and experimental results are presented in Section V. Concluding remarks are in Section VI.

II. Notation and Definitions

A block diagram of a feed-forward filtered-input normalized least mean square (FxNLMS) ANC system is shown in Fig. 1, where $x(n)$ is the acoustic noise signal measured by a reference microphone and is called the reference signal. Noise cancellation is achieved acoustically around an error microphone whose output is $e(n)$. $P(z)$ is the transfer function modeling the primary path. The noise signal after passing through $P(z)$ is called $d(n)$ which is the noise signal to be canceled. The ANC adaptive algorithm determines the noise canceling filter $W(z)$, whose output is $y(n)$. The output of the secondary path $S(z)$ is $y'(n)$. Filter $\hat{S}(z)$ is an estimate of $S(z)$, which we assume errorless, i.e., $\hat{S}(z) \approx S(z)$. The following notation is used in the paper.

NAL	Noise attenuation level.
n	Time (sample) index.
M	Number of subbands.
k	Subband index, $0 \leq k \leq M-1$.
D	Decimation factor used in analysis
L_{p}	Length of the prototype low-pass filter.
$\mathbf{w}$	Weight vector (coefficients) of the FIR noise canceling filter $W(z)$.
N	Length of $\mathbf{w}$.
$\mathbf{w}_k^{\mathrm{SAF}}$	Weight vector for the kth subband filter.
L_{SAF}	Length of each subband adaptive filter.
$W(z)$	z-transform of $\mathbf{w}$.
$W_k^{\mathrm{SAF}}(z)$	z-transform of $\mathbf{w}_k^{\mathrm{SAF}}$.
$((\cdot))_D$	Modulo-D operation.

Bold lower case and bold upper case letters denote vectors and matrices respectively.

III. Delayless Subband ANC Methods

A delayless subband adaptive filtering technique involves the following.[1]

1) A full-band filter that filters the input signal.
2) Decomposition of input and error signals into subbands.
3) Decimation in subbands.
4) Adaptive filters working in subbands.
5) A weight stacking method to combine all subbands weights into a full-band filter.

Signal decomposition is done by analysis filter banks. The adaptive filters operate in subbands and all subband weights are stacked together to make the full-band noise canceling filter $\mathbf{w}$. Stacking in general is done by passing the subband weights through a synthesis filter bank. The analysis and synthesis filter banks must be designed such that they make a perfect reconstruction pair [10]. Fig. 2 shows the delayless subband adaptive filtering scheme used in the ANC FxNLMS algorithm [1]. In this method, $x(n)$ is filtered by $\hat{S}(z)$, generating $x'(n)$. $x'(n)$ and $e(n)$ are then filtered into M subbands named $x'_k(n)$ and $e_k(n)$ using the analysis filter bank $\mathbf{h}(z)$ with a decimation factor D. Filter $\mathbf{h}(z)$ is given by

$$\mathbf{h}(z) = [H_0(z), H_1(z), \ldots, H_{M-1}(z)]^T \tag{1}$$

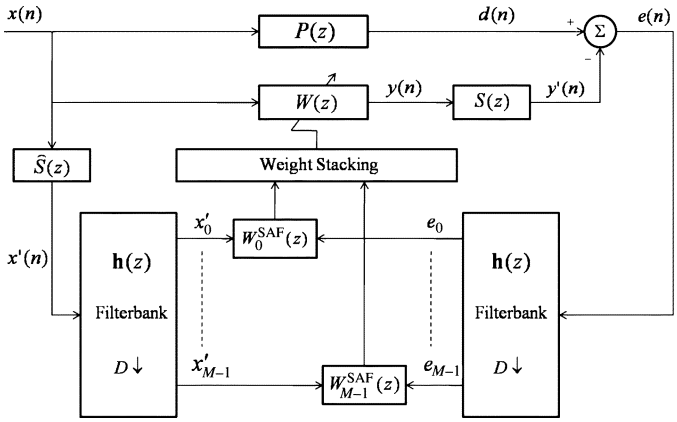

Fig. 2. Feed-forward delayless subband FxNLMS structure.

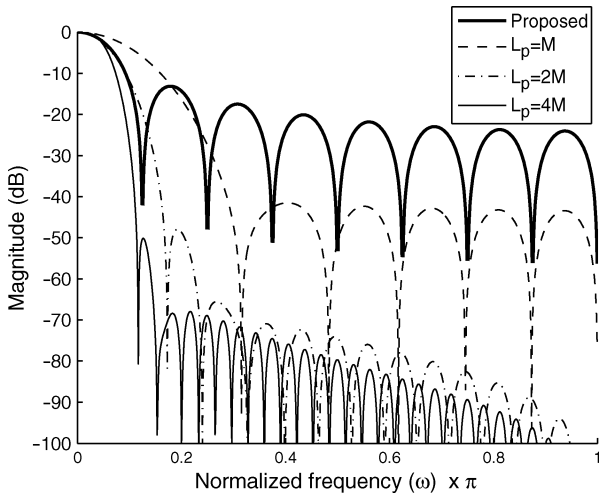

Fig. 3. Low-pass filters designed by Remez algorithm with length $M, 2M$, and $4M$ (thin lines), compared with the frequency response of the proposed filter (bold line) for $M = 16$.

where, $H_k(z)$ is the transfer function of the kth analysis bandpass filter with linear phase and length $L_{\rm p}$. In each subband, weights denoted by $\mathbf{w}_k^{\rm SAF}$ are computed using an adaptive algorithm such as NLMS, i.e.,

$$\mathbf{w}_k^{\rm SAF}(n+1) = \mathbf{w}_k^{\rm SAF}(n) + \mu \frac{\mathbf{x'}^*_k(n) e_k(n)}{\epsilon + \|\mathbf{x'}_k(n)\|^2} \tag{2}$$

where $*$ is the complex conjugation operation, μ is the step size, ϵ is a small positive value, and

$$\mathbf{x'}_k(n) = [x'_k(n), x'_k(n-1), \ldots, x'_k(n - L_{\rm SAF} + 1)]^T \tag{3}$$

$$\mathbf{w}_k^{\rm SAF}(n) = \left[w_{k,1}^{\rm SAF}, w_{k,2}^{\rm SAF}, \ldots, w_{k,L_{\rm SAF}-1}^{\rm SAF}\right]^T. \tag{4}$$

All $\mathbf{w}_k^{\rm SAF}$s are then stacked together to construct $\mathbf{w}$ by employing weight stacking methods. This architecture is delayless since $y(n)$ is not explicitly formed as a combination of subband adaptive filters outputs. The analysis filter banks developed so far have been mainly based on uniform DFT modulated (UDFTM) filter banks [1] and tree structured filter banks like the Hadamard transform [6]. Several methods, such as fast Fourier transform (FFT)-1 [1], FFT-2 [11], DFT-FIR [11], and linear weight transform [12], have been suggested for weight stacking.

UDFTM filter banks are composed of a set of bandpass filters created by modulating a linear phase lowpass (prototype) filter. The low-pass filter has a bandwidth of π/M and the central frequencies of the bandpass filters are at $\omega_k = 2\pi k/M$, for $0 \le k \le M-1$. To exploit the computational advantage of the FFT algorithm, usually M and the length of the low-pass filter are chosen to be powers of 2. The spectral leakage (in-band-aliasing) in the analysis filter banks is minimized when the prototype low-pass filter has a very low stop-band energy [10] and a linear phase with an even-symmetric impulse response [13]. To reduce the stop-band energy for a bandwidth of π/M, the filter order should increase. Fig. 3 compares the frequency responses of such low-pass filters designed for lengths of M, $2M$, and $4M$ for $M = 16$ using the Remez algorithm. As shown for a bandwith of π/M, a low-pass filter of length $4M$ is needed [1]. Since the low-pass filter should have linear phase, its inherent delay increases with M, deteriorating the performance of the SAF algorithm [2], [14]. The effect of delay is more pronounced when the length of $\mathbf{w}$ is increased for primary and secondary paths with long impulse responses. Since long $\mathbf{w}$ requires a lower step size, the adaptive system becomes more sensitive to distortions caused by spectral leakage and delay [14].

The prototype filter design is an optimization problem that jointly minimizes the delay and stop-band energy. These two phenomena are inversely related, i.e., increasing the length of the low-pass filter reduces the spectral leakage and increases the delay and vice versa. The methods used to design such prototype filters are based on quadrature optimization [13], minmax optimization [15], [16], least square[17], and homomorphic filtering [18], [19]. Although, both spectral leakage and delay have direct impact on the delayless SAF performance, our experiments show that the effect of delay is more prominent. Hence, one can tradeoff the spectral leakage for the reduced delay with no performance degradation.

In the next section, a new SAF algorithm based on UDFTM filter banks is presented. The proposed lowpass (prototype) filter in the UDFTM filter banks is of length M and delay $(M-1)/2$, and hence, introduces less delay and side-lobe attenuation than other cases, as shown in Fig. 3. As will be shown, the side-lobe interference is compensated for by oversampling in subbands and proper weight stacking of the subband weights. Unlike existing SAF and BAF algorithms, the proposed SAF algorithm improves the system performance and reduces the computational complexity as M increases.

IV. Proposed SAF Method

In the proposed SAF method, the analysis stage is a UDFTM filter bank. The decimation factor in the filter bank is $M/4$. The bandwidth of the linear-phase low-pass prototype FIR filter is $2\pi/M$. The prototype filter has the length of M introducing a delay of $(M-1)/2$ in the filter banks. This delay is less than the delay presented in the methods of [1] and [6] resulting in the improved performance in our algorithm. The description of the new method is as follows.

A. Proposed Uniform DFT Modulated Filter Bank

Using the UDFTM structure, we propose the following low-pass prototype FIR filter for the filter banks

$$H_0(z) = 1 + z^{-1} + \ldots + z^{-M+1} \tag{5}$$

The resulting filter bank is the simplest FIR perfect reconstruction filter bank [10] which is made by

$$H_k(z) = H_0(ze^{-j2\pi k/M}) \tag{6}$$

with a frequency response of

$$H_0(e^{j\omega}) = \begin{cases} M, & \omega = 0 \\ e^{-j\omega(M-1)/2}\frac{\sin(\omega M/2)}{\sin(\omega/2)}, & \text{otherwise} \end{cases}. \tag{7}$$

The magnitude response of $H_0(e^{j\omega})$ has been plotted in Fig. 3 for $M = 16$. The attenuation of its first side-lobe is about 13 dB relative to its main lobe. The first zero-crossing of $H_0(e^{j\omega})$ is at $2\pi/M$ giving a bandwidth of about $2\pi/M$. Hence, the decimation factor should not exceed $M/2$ in order to avoid spectral aliasing. For the proposed UDFTM filter banks, $h(z)$ is defined by

$$\mathbf{h}(z) = \frac{1}{M}\mathbf{F}^* \begin{bmatrix} 1 \\ z^{-1} \\ \vdots \\ z^{-M+1} \end{bmatrix} \tag{8}$$

where $\mathbf{F}$ is the DFT matrix of order M. The central frequencies of the bandpass filters $H_k(z)$, are located at $\omega_k = 2\pi k/M$ for $0 \le k \le M-1$, which is shown in Fig. 4(a). An important advantage of this UDFTM filter bank is that it can be realized using a tapped delay line of length M followed by an inverse FFT block.

The $H_0(z)$ in (5) has linear phase with a delay of $(M-1)/2$. By choosing (5), the delay in UDFTM filter bank and attenuation of side-lobes are less than those given in [1], [6]. To alleviate the interference of the side-lobes on the system performance, we choose an appropriate decimation factor and perform the weight stacking as follows. We note that oversampling in subbands helps to mitigate the spectral aliasing caused by the side-lobes during the decimation operation. In our approach, the decimation factor is chosen to be $D = M/4$. After decimation by a factor of $M/4$, only the side-lobes in intervals of $[8\pi k/M, 10\pi k/M]$ (for $M \ge 8$, see Fig. 3) interfere with the main-lobe over the interval $[0, \pi/2]$. Since these side-lobes are attenuated by more than 20 dB, the interference in the main-lobe reduces more than 7 dB (compared to 13 dB from the first side-lobe).

As a direct result of using a decimation factor of $D = M/4$, the bandpass filters with the same values of $((k))_4$ will have the same spectra. Hence, there are four types of output spectra which are used to design an appropriate weight stacking method. The concept is illustrated in Fig. 4(b)–(e), where a triangular spectrum is used to symbolically represent the spectrum of each bandpass filter given by (6).

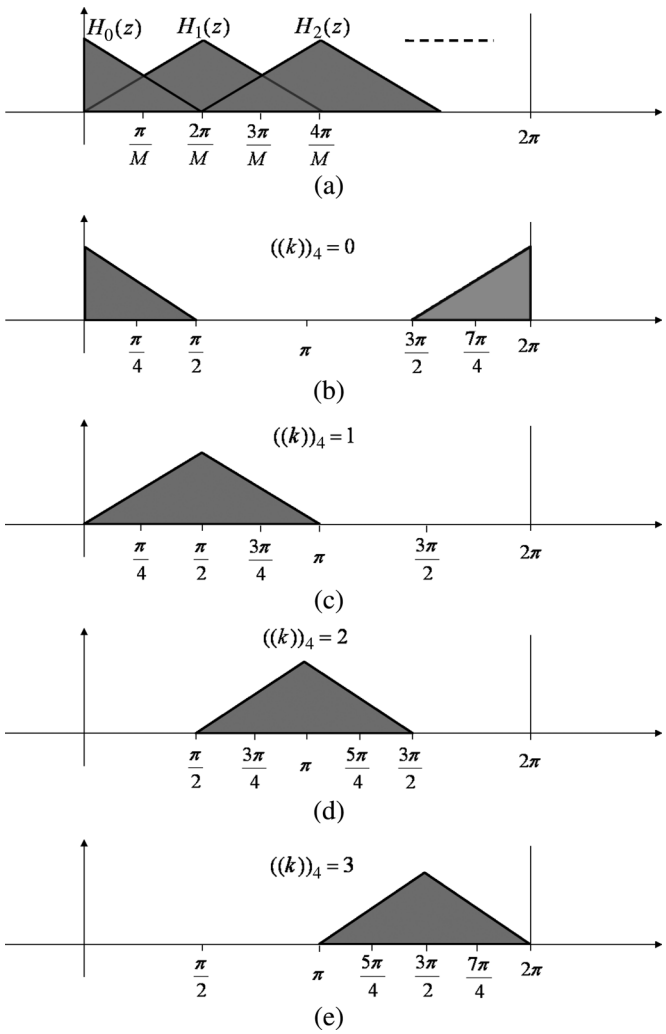

Fig. 4. Symbolic representation of spectra. (a) Frequency response of UDFT filter bank. After decimation by $D = M/4$, the spectral shapes change according to the subband index k, i.e., (b) $((k))_4 = 0$, (c) $((k))_4 = 1$, (d) $((k))_4 = 2$, (e) $((k))_4 = 3$.

B. Proposed Weight Stacking Method

Among the synthesis filter banks commonly used for weight stacking are the computationally efficient delayless methods of FFT-1 [1] and FFT-2 [11]. In these methods, the DFT bins of $\mathbf{w}$, denoted by $W[\cdot]$, are divided equally among M subbands. Since the DFT bins of $\mathbf{w}$ of length N, are uniformly distributed in $[0, 2\pi)$, i.e. $2\pi l/N$ for $0 \le l \le N-1$, each subband contributes to N/M bins of $W[\cdot]$. The bins of $W[\cdot]$ in the kth subband are selected from the DFT bins of the kth subband weight, denoted by $W_k^{\mathrm{SAF}}[\cdot]$, and $\mathbf{w}$ is reconstructed by computing the inverse DFT of $W[\cdot]$. Bin selection is done based on the relation between the frequency response of $\mathbf{w}$ and $\mathbf{w}_k^{\mathrm{SAF}}$.

As shown in Fig. 4(a), the central frequencies of the UDFTM bandpass filters are located at $\omega_k = 2\pi k/M$. The corresponding $H_k(z)$ has the bandwidth of $2\pi/M$ and $4\pi/M$ for $k = 0$ and $k \ne 0$, respectively, and the adjacent bandpass filters share a bandwidth of $2\pi/M$. After decimation by $D = M/4$, the spectral shapes of $Y_k(e^{j\omega})$ and $E_k(e^{j\omega})$ resemble those shown in

Fig. 4(b)–(e), depending on the value of $((k))_4$. The resultant $W_k^{\mathrm{SAF}}(e^{j\omega})$ follows the same spectral pattern too.

As illustrated in Fig. 4(a)–(e), the bins of $W[\cdot]$ are selected as follows.

1) For the interval $[0, \pi/M)$, they are equal to the bins of $W_0^{\mathrm{SAF}}[\cdot]$ in the interval $[0, \pi/4)$.
2) For the interval $[(2k-1)\pi/M, (2k+1)\pi/M)$ and $((k))_4 = 0$, they are equal to the bins of $W_k^{\mathrm{SAF}}[\cdot]$ in the interval $[7\pi/4, 2\pi)$ and $[0, \pi/4)$.
3) For the interval $[(2k-1)\pi/M, (2k+1)\pi/M)$ and $((k))_4 = 1$, they are equal to the bins of $W_k^{\mathrm{SAF}}[\cdot]$ in the interval $[\pi/4, 3\pi/4)$.
4) For the interval $[(2k-1)\pi/M, (2k+1)\pi/M)$ and $((k))_4 = 2$, they are equal to the bins of $W_k^{\mathrm{SAF}}[\cdot]$ in the interval $[3\pi/4, 5\pi/4)$.
5) For the interval $[(2k-1)\pi/M, (2k+1)\pi/M)$ and $((k))_4 = 3$, they are equal to the bins of $W_k^{\mathrm{SAF}}[\cdot]$ in the interval $[5\pi/4, 7\pi/4)$.
6) For the interval $[2\pi - \pi/M, 2\pi)$, they are equal to the bins of $W_{M-1}^{\mathrm{SAF}}[\cdot]$ in the interval $[7\pi/4, 2\pi)$.

The bin selection is based on the spectral shapes exemplified in Fig. 4(a)–(e), and the fact that the bins are distributed among the subbands proportional to their bandwidths. Mathematically, the proposed DFT bin selection and stacking methods are expressed as follows.

Proposed FFT-1 weight stacking method (PFFT-1)

$$\begin{cases} l \in [0, N/2], & W[l] = W^{\mathrm{SAF}}_{((\lfloor \frac{lM}{N} \rfloor))_M} \left[((l))_{\frac{4N}{M}} \right] \\ l \in (N/2, N), & W[l] = W[N-1]^* \end{cases}. \quad (9)$$

Proposed FFT-2 weight stacking method (PFFT-2)

$$\begin{cases} l \in [0, N], & W[l] = W^{\mathrm{SAF}}_{((\lfloor \frac{lM}{2N} \rfloor))_M} \left[((l))_{\frac{8N}{M}} \right] \\ l \in (N, 2N), & W[l] = W[2N-l]^* \end{cases}. \quad (10)$$

The PFFT-2 method uses twice as many DFT points than that of PFFT-1, which results in reduced weight stacking distortion [20]. Furthermore, unlike the original methods of FFT-1 [1] and FFT-2 [11], the frequency responses of PFFT-1 and PFFT-2 do not have nulls at $\omega = \pi$, resulting in improved performance of the ANC system. In the proposed methods, the length of each subband adaptive filter should be at least $L_{\mathrm{SAF}} = 4N/M$ for PFFT-1 and $L_{\mathrm{SAF}} = 2N/M$ for PFFT-2, since only one fourth of the total DFT bins in each subband are transformed. The PFFT-2 uses zero-padding to compute a DFT of size $2L_{\mathrm{SAF}}$.

V. Computational Complexity

The computational complexity of the proposed subband filtering technique is calculated by counting the number of real multiplications required for the following operations.

1) Decimation by the factor $D = M/4$.
2) Calculation of the $M/2+1$ filter bank outputs. Only $M/2+1$ subbands are considered since $\mathbf{w}$ is real.
3) Weight update operation for calculating $M/2+1$ adaptive filters.
4) Weight stacking and calculation of $\mathbf{w}$ which includes $M/2+1$ FFT operations to compute $W_k^{\mathrm{SAF}}[\cdot]$s and an IFFT operation to compute $\mathbf{w}$.

TABLE I
Computational Complexity for the Proposed Method in Terms of Number of Real Multiplications Per Input Sample

Algorithm	Number of real multiplications†
Proposed UDFT	$4\log_2 M$
NLMS to compute $\mathbf{w}_k^{\mathrm{SAF}}$	$(1+\frac{2}{M})\left(\frac{8N}{M}\right)$
PFFT-1	$\frac{4N}{M}\left[(2+\frac{4}{M})\left(\log_2 \frac{4N}{M}\right) + \log_2 N\right]$
PFFT-2	$\frac{8N}{M}\left[(2+\frac{4}{M})\left(\log_2 \frac{8N}{M}\right) + \log_2 2N\right]$

† Computed for $M/2+1$ subbands with the decimation factor of $D = M/4$.

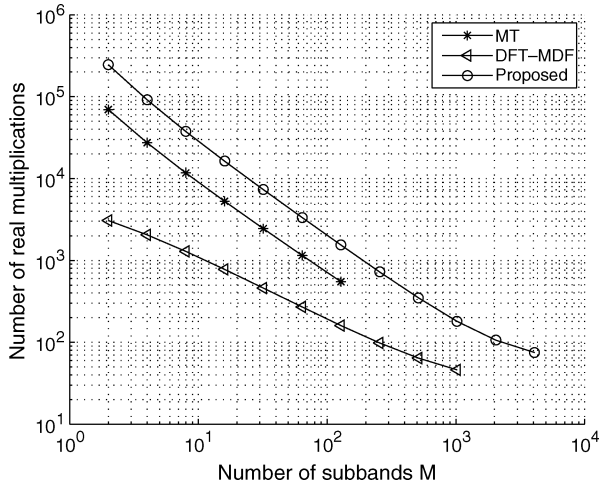

Fig. 5. Comparison of computational complexity per input sample versus number of subbands (M), for $N = 1024$. MT diverges for $M > 128$.

Table I summarizes the computational complexity per input sample for the operations listed above. The total complexity is plotted in Fig. 5 versus the number of subbands M. The plot is for the PFFT-2 method with $L_{\mathrm{SAF}} = 4N/M$, as it results in better performance than that of PFFT-1. For comparison purposes, we have included the computational complexity of the MT [1] and DFT-MDF [2] algorithms in Fig. 5. As shown, the computational complexities of all methods reduce almost exponentially with M. The proposed technique compared to the other methods for small values of M has higher computational complexity. However, as it will be discussed in Section V, the new technique works very well with a larger number of subbands, improving the system performance and attaining lower complexity, whereas the MT method fails to converge and the performance of the DFT-MDF method deteriorates.

VI. Experimental Results

For the system shown in Fig. 2, the noise attenuation level is calculated by

$$\mathrm{NAL}(n) = 20\log_{10}\left(\frac{\|d(m)\|_2}{\|e(m)\|_2}\right)$$
$$n - \frac{L_{\mathrm{f}}}{2} < m \le n + \frac{L_{\mathrm{f}}}{2} \quad (11)$$

where L_{f} is the frame length, and is the ratio of the norms of the noise $d(n)$ and the error $e(n)$ at the canceling point after the ANC adaptive algorithm has converged. Since white noise is not

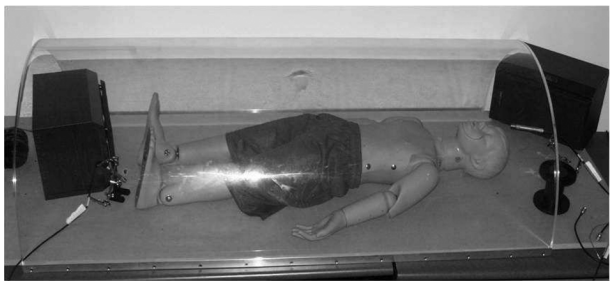

Fig. 6. Test bed used to measure $P(z)$ and $S(z)$. The targeted application is active noise cancelation of the acoustic noise in MRI machines.

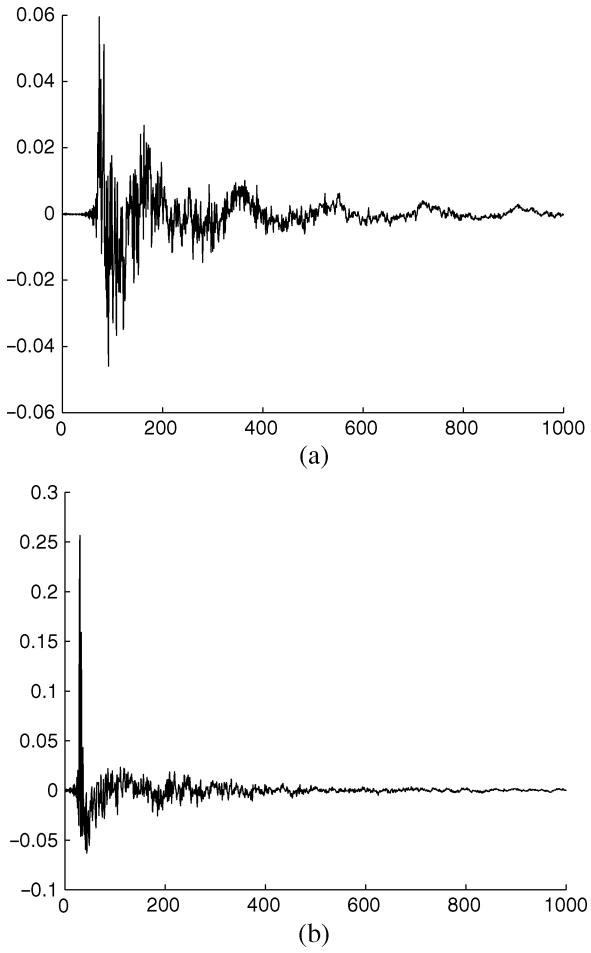

Fig. 7. Measured actual impulse responses (a) Primary path $P(z)$. (b) Secondary path $S(z)$.

predictable, it is usually used as a worst case test of ANC systems. The performance of the proposed algorithm is evaluated and compared to those of the MT and DFT-MDF algorithms using a zero-mean unit-variance white noise as the input signal. A series of simulations were conducted to evaluate the performance of an ANC system using the proposed subband filtering technique. For this purpose, transfer functions of the primary and secondary paths were measured for a test bed using the large half-cylindrical tube shown in Fig. 6. Fig. 7 shows the measured impulse responses of the primary and secondary paths. The experiment was to run the ANC system in Fig. 2 with the measured

TABLE II
MAXIMUM ATTAINABLE VALUE OF NAL AND ITS CORRESPONDING VALUE OF M FOR DIFFERENT ADAPTIVE FILTERING ALGORITHMS. $N = 1024$

Algorithms	Max. NAL (dB)	M	Complexity
Proposed	17.92	1024	184
MT	14.82	64	1149
DFT-MDF	17.88	16	778

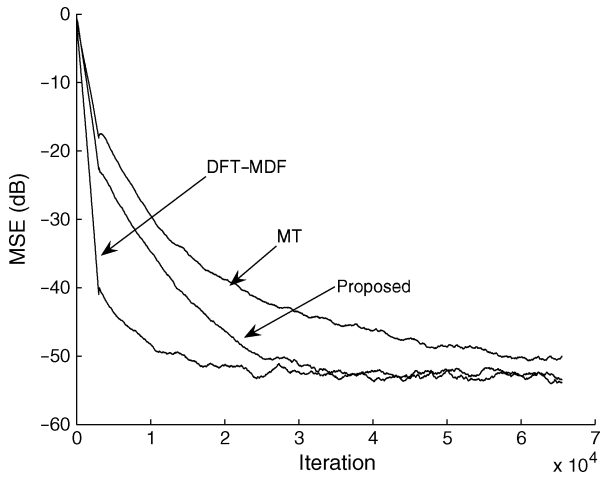

Fig. 8. MSE decay versus time sample for the MT, DFT-MDF, and the proposed methods for the best operating conditions given in Table II.

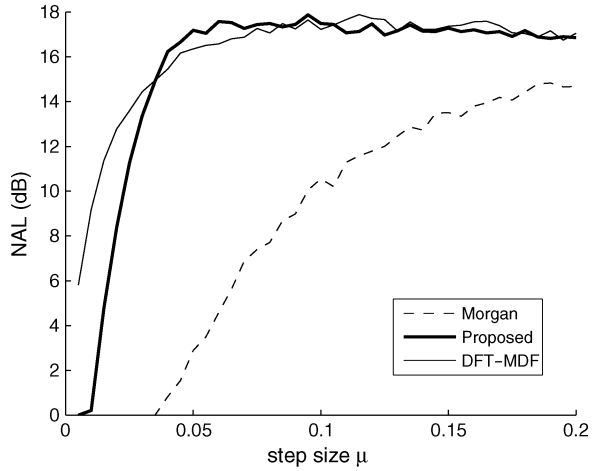

Fig. 9. NAL versus step size μ, for the MT, DFT-MDF, and the proposed methods, using the best operating conditions given in Table II.

$P(z)$ and $S(z)$ for 2^{16} samples of white input noise and measure the output NALs and MSE curves for each algorithm. The experiment was repeated for different values of N, M, and step size μ. The final results were calculated by averaging over 100 independent runs. The value $N = 1024$ resulted in the highest NAL value. The maximum obtainable value of NAL and corresponding value of M were chosen as the best operating condition for each algorithm in our experiments. The results are shown in Table II. The proposed method achieves 17.92 dB of noise reduction with $M = 1024$ subbands resulting in much lower complexity than the other two methods.

As shown in Fig. 8, the convergence rate of the proposed algorithm with PFFT-2 is faster than that of the MT algorithm. The DFT-MDF has an initial fast convergence rate that slows

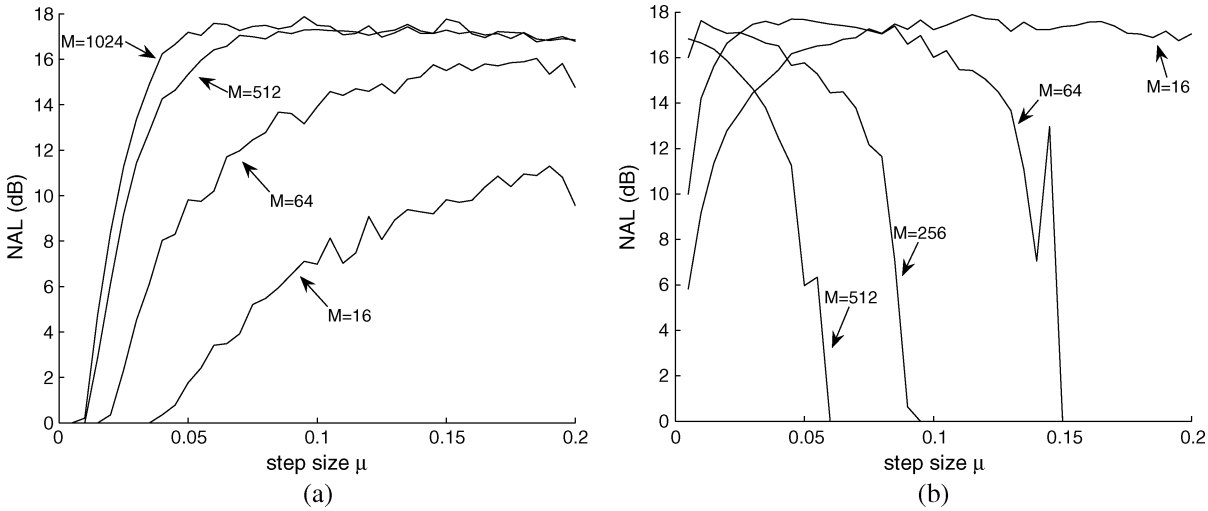

Fig. 10. Comparing NAL versus step size μ of (a) proposed method, (b) and DFT-MDF, for different numbers of subbands (M).

down after some time. The proposed method compared to the DFT-MDF method has slower convergence but they both reach steady state values almost simultaneously. The fast initial convergence rate of DFT-MDF method is due to the fact that its UDFTM filter bank is the eigenmatrix of the blocks processed by the DFT-MDF algorithm [2].

Fig. 9 shows the maximum achievable NAL values versus μ for the proposed, MT, and DFT-MDF algorithms. The plots are for the values of M given in Table II. As shown, the MT method is very sensitive to the step-size value: a small change in μ reduces the maximum achievable value of NAL. The MT method diverges for $\mu > 0.2$ in our experiments. Conversely, the proposed and the DFT-MDF algorithms show significant robustness to variations of μ. Fig. 10 compares the NAL variation of the proposed and DFT-MDF methods for different numbers of subbands. As shown, the robustness of the proposed algorithm increases with M, while the DFT-MDF algorithm becomes more sensitive to variations of μ. The proposed method works very well for a large number of subbands. It achieves its maximum performance (i.e., maximum NAL value) at $M = 1024$, reducing the computational complexity drastically. However, The MT algorithm diverges for $M > 128$. Although the DFT-MDF works with a large number of subbands, but it becomes more sensitive to μ, as shown in Fig. 10(b), and a small change in μ degrades its performance significantly.

VII. Conclusion

Acoustic paths such as those encountered in ANC application usually have long impulse responses, which require longer adaptive filters for noise cancellation. Subband adaptive filters working with a large number of subbands has been shown to be a good solution to this problem. The focus of this paper was to design such a high-performance SAF algorithm. The performance limiting factors of existing SAF structures were found to be due to the inherent delay and side-lobes of the prototype filter in the analysis filter banks. Hence, the analysis filter banks were modified to reduce the inherent delay. A new weight stacking transform was designed to alleviate the interference introduced by the side-lobes. The modifications resulted in a new subband method that, unlike existing methods, improves the performance and reduces the computational complexity for a large number of subbands. Experimental results showed that the proposed method outperformed the two commonly used SAF and BAF methods.

References

[1] D. R. Morgan and J. C. Thi, "A delayless subband adaptive filter architecture," *IEEE Trans. Signal Process.*, vol. 43, no. 8, pp. 1819–1830, Aug. 1995.

[2] R. Merched and A. H. Sayed, "An embedding approach to frequency-domain and subband adaptive filtering," *IEEE Trans. Signal Process.*, vol. 48, no. 9, pp. 2607–2619, Sep. 2000.

[3] P. Loizou, *Speech Enhancement: Theory and Practice*. Boca Raton, FL: CRC, 2007.

[4] V. R. Ramachandran, G. Kannan, A. A. Milani, and I. M. S. Panahi, "Speech enhancement in functional MRI environment using adaptive sub-band algorithms," in *Proc. ICASSP'07*, 2007, pp. II-341–II-344.

[5] P. Loizou and K. Kokkinakis, "Subband-based blind signal processing for source separation in convolutive mixtures of speech," in *Proc. ICASSP'07*, 2007, pp. IV-917–IV-920.

[6] N. Hirayamaa, H. Sakai, and S. Miyagi, "Delayless subband adaptive filtering using the hadamard transform," *IEEE Trans. Acoust., Speech, Signal Process.*, vol. 47, pp. 1731–1734, Jun. 1999.

[7] P. Eneroth, "Joint filterbanks for echo cancellation and audio coding," *IEEE Trans. Speech Audio Process.*, vol. 11, no. 4, pp. 342–354, Jul. 2003.

[8] D. Zhou and V. DeBrunner, "A new active noise control algorithm that requires no secondary path identification based on the SPR property," *IEEE Trans. Signal Process.*, vol. 55, no. 5, pp. 1719–1729, May 2007.

[9] J. Shynk, "Frequency-domain and multirate adaptive filtering," *IEEE Signal Process. Mag.*, vol. 9, no. 1, pp. 14–37, Jan. 1992.

[10] P. Vaidyanathan, *Multirate Systems and Filter Banks*. Englewood Cliffs, NJ: Prentice-Hall, 1993.

[11] J. Huo, S. Nordholm, and Z. Zang, "New weight transform schemes for delayless subband adaptive filtering," in *Proc. GLOBECOM'01*, New York, Nov. 2001, pp. 197–201.

[12] L. Larson, J. de Haan, and I. Claesson, "A new subband weight transform for delayless subband adaptive filtering structures," in *Proc. Digital Signal Process. Workshop*, Aug. 2002, pp. 201–206.

[13] J. M. de Haan, N. Grbic, I. Claesson, and S. E. Nordholm, "Filter bank design for subband adaptive microphone arrays," *IEEE Trans. Speech Audio Process.*, vol. 11, no. 1, pp. 14–23, Jan. 2003.

[14] A. H. Sayed, *Fundamentals of Adaptive Filtering*. New York: Wiley, 2003.

[15] Z. Lin and Y. Liu, "Design of complex fir filters with reduced group delay error using semidefinite programming," *IEEE Trans. Signal Process.*, vol. 13, no. 9, pp. 529–532, Sep. 2006.

[16] R. Venkataramani and Y. Bresler, "Filter design for MIMO sampling and reconstruction," *IEEE Trans. Signal Process.*, vol. 51, no. 12, pp. 3164–3167, Dec. 2003.

[17] Y. C. Lim, J. Lee, C. K. Chen, and R. Yang, "A weighted least squares algorithm for quasi-equiripple FIR and IIR digital filter design," *IEEE Trans. Signal Process.*, vol. 40, no. 3, pp. 551–558, Mar. 1992.
[18] H. Gustafsson, S. E. Nordholm, and I. Claesson, "Spectral subtraction using reduced delay convolution and adaptive averaging," *IEEE Trans. Speech Audio Process.*, vol. 9, no. 8, pp. 799–807, Nov. 2001.
[19] A. V. Oppenheim and R. W. Schafer, *Discrete-Time Signal Processing*, 2nd ed. Englewood Cliffs, NJ: Prentice-Hall, 1999.
[20] A. A. Milani, G. Kannan, I. Panahi, R. Briggs, and K. Gopinath, "Weight stacking analysis of delayless subband adaptive algorithms for fMRI active noise cancellation," in *Proc. IEEE Dallas EMBS Workshop*, Dallas, Nov. 2007, pp. 134–137.

Ali A. Milani received the B.S. degree in electrical engineering from the Sharif University of Technology, Tehran, Iran, in 2001 and the M.S. degree from the School of Electrical Engineering and Computer Science, University of Texas at Dallas, Richardson, in 2007, where he is currently pursuing the Ph.D. degree.

His research interests are audio, speech and multimedia signal processing, and embedded multimedia systems. Since 2005, as a member of the Statistical Signal Processing Research Lab, he has been working on adaptive noise cancellation, speech enhancement, and microphone arrays.

Mr. Milani is the recipient of the outstanding paper awards from the Acoustical Society of America and Analog Devices, Inc.

Issa M. S. Panahi (S'84–M'88–SM'07) received the Ph.D. degree in electrical engineering from the University of Colorado at Boulder in 1988.

He joined the faculty of the University of Texas at Dallas (UTD), Richardson, after working in industry for several years, and he is now an Assistant Professor in the Department of Electrical Engineering. He is a Director of the Statistical Signal Processing and Acoustic Research Laboratories at UTD. His research areas of interest include MIMO digital signal processing, source separation, signal estimation, system identification, noise cancellation, speech enhancement, and embedded DSP systems. He was a Research Scientist in the Geophysical Signal Processing Group at Bellaire Research Lab, Shell Oil Development, Houston, TX (1988-1991), and a DSP Chief Architect, Worldwide Applications Manager, Senior Member Of The Technical Staff, Chief Technology Officer, and Advance Systems Development Manager in the embedded DSP systems business unit at Texas Instruments, Inc., in Houston, (1991- 2000). He was an Application Manager with the Wireless/OMAP Group, Texas Instruments, Dallas, before joining UTD in 2001. He holds one US patent. He is author/coauthor of several Texas Instruments books, and has published numerous conference, journal, and technical papers.

Dr. Panahi cofounded the IEEE-Dallas Chapter of Engineering in Medicine and Biology Society (EMBS) in 2006. He has been Vice-Chair of the IEEE-Dallas Chapters of the EMBS and Signal Processing (SP) Societies since 2006. He was the Secretary and Treasurer (2004), and Program Chair (2005) of the IEEE Signal Processing chapter in Dallas. He was recipient of the "2005 Outstanding Service Award" from the Dallas Section of the IEEE.

Philipos C. Loizou received the B.S., M.S., and Ph.D. degrees, all in electrical engineering, from Arizona State University (ASU), Tempe, in 1989, 1991, and 1995, respectively.

From 1995 to 1996, he was a Postdoctoral Fellow in the Department of Speech and Hearing Science at ASU, working on research related to cochlear implants. He was an Assistant Professor at the University of Arkansas at Little Rock from 1996 to 1999. He is now a Professor and holder of the Cecil and Ida Green Chair in the Department of Electrical Engineering, University of Texas at Dallas, Richardson. His research interests are in the areas of signal processing, speech processing, and cochlear implants. He is author of the book *Speech Enhancement: Theory and Practice* (CRC, 2007).

Dr. Loizou is currently an Associate Editor of the IEEE TRANSACTIONS ON BIOMEDICAL ENGINEERING and the *International Journal Of Audiology*. He was an Associate Editor of the IEEE TRANSACTIONS ON SPEECH AND AUDIO PROCESSING (1999-2002) and the IEEE SIGNAL PROCESSING LETTERS (2006-2008). He is currently a member of the Speech Technical Committee of the IEEE Signal Processing Society.